

# IV-tuning: Parameter-Efficient Transfer Learning for Infrared-Visible Tasks

Yaming Zhang<sup>1</sup> Chenqiang Gao<sup>1,2\*</sup> Fangcen Liu<sup>1</sup> Junjie Guo<sup>1</sup> Lan Wang<sup>3</sup> Xinggan Peng<sup>4</sup>  
Deyu Meng<sup>5</sup>

<sup>1</sup> Chongqing University of Posts and Telecommunications <sup>2</sup> Sun Yat-sen University <sup>3</sup> Michigan State University  
<sup>4</sup> Nanyang Technological University <sup>5</sup> Xi'an Jiaotong University

{YummyZhang1989, liufc67, gjj893866738}@gmail.com, gaochq6@mail.sysu.edu.cn,  
wanglan3@msu.edu, xinggan001@entu.edu.sg, dymeng@mail.xjtu.edu.cn

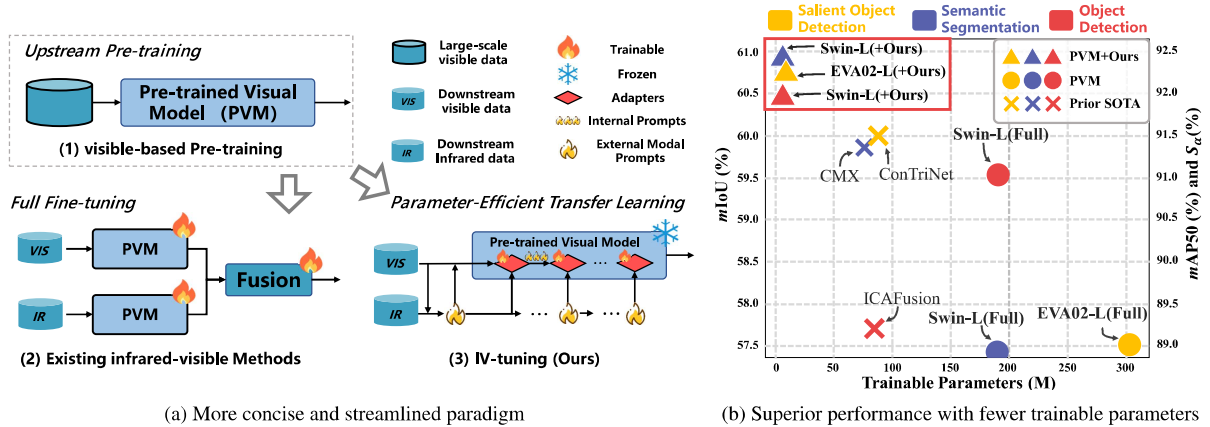


Figure 1. We demonstrate the superiority of the proposed method in both paradigm and performance, as illustrated. (a) (1): Pre-trained Visual Models (PVMs) are powerful pre-trained models that serve as robust backbones. (a) (1)→(2): Existing infrared-visible methods typically extend visible-based models into a dual-branch network and perform fine-tuning. (a) (1)→(3): We propose a more concise and streamlined framework for the parameter-efficient adaptation of visible-based VFMs to various infrared-visible tasks, including salient object detection, semantic segmentation and object detection. (b) Our proposed method achieves superior performance with fewer trainable parameters compared to previous state-of-the-art methods and PVMs.

## Abstract

Various infrared-visible (IR-VIS) tasks greatly benefit from the advantage of combining infrared and visible modalities. Driven by the motivation that **streamlining the infrared flow and harnessing PVMs with fewer parameters for superior performance**, we propose “**IV-tuning**”, a novel and general fine-tuning approach, to parameter-efficiently harness PVMs for various infrared-visible downstream tasks. At its core, *IV-tuning* freezes pre-trained visible-based<sup>1</sup> PVMs and integrates infrared flow into modal prompts to interact with adapters, which achieves a more efficient and general modal interaction paradigm. By fine-tuning approximately 3% of the backbone parameters, *IV-tuning* outperforms full fine-tuning and

previous state-of-the-art methods across multiple baselines in multiple tasks, including IR-VIS salient object detection, semantic segmentation and object detection. Extensive experiments demonstrate that *IV-tuning* achieves superior performance with fewer trainable parameters, providing a good alternative to full fine-tuning and a novel method of extending visible-based models for infrared-visible tasks. The code will be provided in supplementary material.

## 1. Introduction

In Computer Vision (CV), various tasks, such as salient object detection, semantic segmentation and object detection, have predominantly relied on the visible modality, and numerous visible-based methods [22, 53, 62, 65, 75, 79, 83] have spurred over the past decades. However, the perfor-

<sup>1</sup>Denotes training based on visible-modality data.

mance of visible-based methods degrades in challenging scenarios (e.g., nighttime, fog, rain) due to the inherent limitations of visible imaging principles. Therefore, leveraging the infrared and visible images with strong complementary information to improve performance has increasingly drawn attention. Various methods [16, 32, 38, 51, 55, 77, 78] have been widely explored for the infrared-visible tasks with classic backbones, such as ResNet [18], VGGNet [52] and CSPDarkNet [1].

With the introduction of the Transformer [60], transformer-based Pre-trained Visual Models (PVMs), such as ViT [12], Swin Transformer [39], MAE [19], EVA02 [14] and DINOv2 [45] have demonstrated powerful generalization across various downstream tasks. Some infrared-visible methods [40, 51, 77] have begun to leverage the general representations of PVMs to improve performance. As illustrated in Figure 1 (a) (1)→(2), these methods usually introduce the same or slightly lighter-weight backbones for the infrared modality, and design fusion modules to integrate the complementarity of the two modalities. Subsequently, the entire model is fine-tuned on task-specific datasets. Albeit effective, they also expose some limitations: 1) *Complex fusion networks are designed task-specifically, which lack generalization [13, 16, 32, 49].* 2) *Domain differences exist between infrared data and visible data used for pre-training [36]. Meanwhile, the commonly used infrared-visible datasets, such as MSRS [57] and M3FD [37], are significantly smaller than those used for pre-training, such as ImageNet [10] and LVD-142M [45]. When fine-tuning on limited datasets, the well-trained knowledge space of the PVMs could be disrupted [11, 48], resulting in inferior performance.* 3) *The full fine-tuning process is resource-intensive, time-consuming, and inefficient, particularly with dual-branch models, making it impractical for numerous applications and transfer deployments.* Hence, in the current trend of leveraging powerful transformer-based PVMs, one intuitive question emerged: ***Can we simplify the way of utilizing the infrared modality, and harness one visible-based PVMs for IR-VIS tasks in a more efficient and general way?***

Parameter-Efficient Transfer Learning (PETL) methods are quickly introduced to Computer Vision due to their notable success in Natural Language Processing (NLP), such as prompt-tuning [26, 29, 47] and adapter-tuning [5, 31, 81]. By freezing the backbone and fine-tuning only a small portion of the parameters, these methods have demonstrated that the general representations of PVMs can be transferred to downstream tasks more effectively. A more challenging task, however, is to simultaneously harmonize the efficient harness of inter-modal information and the adaptation of PVMs to downstream tasks.

In this work, we present *IV-tuning*, a novel and general parameter-efficient transfer learning framework designed

to adapt the visible-based Pre-trained Visual Models for infrared-visible downstream tasks, including salient object detection, semantic segmentation and object detection. As illustrated in Fig. 1 (a) (1)→(3), instead of adding an extra backbone branch, IV-tuning freezes the entire backbone of the PVMs and introduces modal prompts to the tuning process, which inherits the general representations of PVMs to the maximum extent. Built upon the robust and stable visible features extracted by the PVMs, the infrared modality serves as auxiliary information and is encoded into the modal prompts, which learns to align with the visible features to facilitate inter-modal learning. Specifically, we propose the External Modal Prompt Generator (EMPG) to generate prompts enriched with dual-modal information, which are then fused with the visible input and fed into transformer-based PVMs. Tailored for dense predictions tasks, we propose the Hybrid Adapter (HA) to effectively transfer visual knowledge from PVMs. Simultaneously, the Internal Prompt Adapter (IPA) refines the external prompts into internal prompts, reducing heterogeneous feature conflicts when prompting backbone feature stream, and reinforcing low-level features extracted in the early stages. This process effectively harmonizes the balance between upstream representations and downstream tasks, and achieves an efficient and general way for the infrared modality to complement the visible features. The main contributions of our work can be summarized below:

- We present IV-tuning, a novel and general framework for parameter-efficient fine-tuning Pre-trained Visual Models (PVMs). Benefiting from modal prompts and adapters, the easily accessible PVMs can be effectively adapted to various infrared-visible tasks, including salient object detection, semantic segmentation, and object detection.
- We propose the External Modal Prompt Generator, Hybrid Adapter, and Internal Prompt Adapter, which are used for valid modal prompts generation, features adaptation, and prompts transformation, respectively. The infrared modality is streamlined into prompts instead of introducing an extra backbone.
- Extensive experiments demonstrate the effectiveness of IV-tuning. By training approximately 3% of the parameters in PVMs, IV-tuning achieves superior performance in IR-VIS salient object detection, semantic segmentation and object detection, outperforming the full fine-tuning paradigm and previous state-of-the-art methods, as shown in Fig. 1 (b).

## 2. Related Work

### 2.1. Infrared-visible Tasks.

For advancing performance specifically in semantic segmentation, object detection or salient object detection, existing infrared-visible methods mainly adopt two kinds of

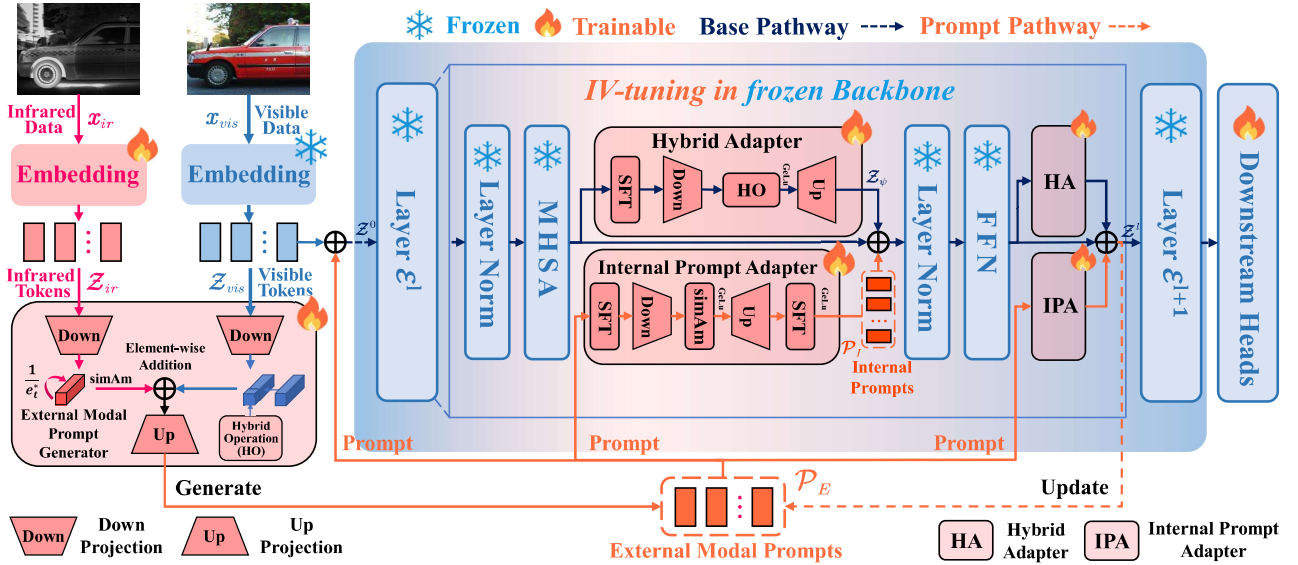


Figure 2. **The overview of the proposed IV-tuning.** IV-tuning freezes the  $L$ -layer transformer-based backbone and only fine-tunes a select few modules. The learned external modal prompts  $\mathcal{P}_E$  are injected into each encoder layer to generate internal prompts  $\{\mathcal{P}_i^l\}_{i=1}^L$ , with each encoder layer’s outputs updating the external modal prompts. IV-tuning integrates adapter-tuning with prompt-tuning to collaboratively learn inter-modal complementarity while effectively adapting Pre-trained Visual Models to infrared-visible downstream tasks.

approaches: (1) performing image-level fusion, and feeding the fused image into specific networks [27, 51, 77], and (2) designing end-to-end frameworks tailored for specific task [15, 16, 32, 33, 66]. Whether training a designed network from scratch or fully fine-tuning a pre-trained model, these methods routinely add an extra backbone, where the infrared backbone can only load visible-based parameters during fine-tuning. For example, CDDFuse [77] introduced a dual-branch Transformer-CNN feature extractor and performed a two-stage training method for semantic segmentation. ICAFuse [51], utilized a dual-branch cross-attention transformer to enhance feature discriminability for objection detection. Similarly, SwinNet[40] built dual-branch Swin Transformer for the salient object detection. Although effective, these dual-branch architectures limit the ability to harness large-scale PVMs for infrared-visible tasks. Moreover, these methods are mostly task-specific, thus lacking generalization across different tasks. In this paper, we aim to explore a novel, efficient, and effective approach, without introducing an additional backbone for infrared modality, to perform infrared and visible tasks, including salient object detection, semantic segmentation and object detection.

## 2.2. Pre-trained Visual Models.

Early models [18, 23, 25, 52, 54, 68] are usually pre-trained on the Imagenet-1K dataset and fine-tuned on downstream tasks, enabling faster convergence and improved performance. As the transformer [60] rises, larger visual

models (e.g., ViT [12] and Swin Transformer [39]) are pre-trained on larger datasets (e.g., ImageNet-21K [10] or JFT-3B [73]), demonstrating superior scalability, long-range dependency modeling, and representation learning capabilities compared to CNNs. Some of them, known as the Vision Foundation Models, are pre-trained in a self-supervised or semi-supervised manner [2], such as MAE [20], which employs masked image modeling for self-supervised learning, and EVA02 [14], conduct masked image modeling distillation learning by using a multi-modal visual encoder as the teacher. These PVMs have shown strong generalization across various downstream tasks [35, 36, 64]. However, few works have studied the efficient execution of IR-VIS tasks by only utilizing one larger and more powerful PVM.

## 2.3. Visual Parameters Efficient Transfer Learning.

With the rise of PVMs, efficiently adapting these large-scale models has drawn much attention. Parameter-Efficient Transfer Learning (PETL) offers a compelling alternative to full fine-tuning by freezing the backbone and optimizing only a few parameters. Prompt-tuning [26, 29, 47, 82] introduces learnable prompts in the input space, and adapter-tuning [5, 31, 71] inserts lightweight bottlenecks into the transformer encoder. Both paradigms can achieve performance on par with or surpass that of fully fine-tuning with fewer parameters. However, most existing methods either focus on efficiently fine-tuning one single task or remain confined to a single modality [5, 26, 31, 47, 65, 82]. In

multi-modal field, a representative work is ViPT [82], which designed a modal complementary prompter to introduce multiple modalities into the ViT-based RGB tracker. However, we found that it is not applicable in our image-level scenario. In contrast, we aim to integrate prompt-tuning and adapter-tuning within a broader range of pre-trained visual models, achieving superior IR-VIS tasks generally and efficiently.

### 3. Methodology

#### 3.1. Overall Architecture

Compared to visible tasks, the infrared-visible tasks introduce an extra infrared input  $\mathbf{x}_{ir}$ , which is temporally synchronized and spatially aligned with the visible input  $\mathbf{x}_{vis}$ . These tasks aim to learn the mapping function  $F$ :

$$\mathbf{p} = F[\phi(f(\mathbf{x}_{vis}, \mathbf{x}_{ir}))], \quad (1)$$

where  $\mathbf{p}$  is the prediction result,  $\phi$  is a task-oriented head, and  $f$  is a transformer-based Pre-trained Visual Models (PVMs). As shown in Fig. 2, we introduce an independent patch embedding layer for the infrared data, mapping the input image  $\mathbf{x}_{ir}$  to tokens of the same dimension  $D$  as the visible modality:  $\mathcal{Z}_{ir} \in \mathbb{R}^{N \times D}$ , where  $N$  is the token length. Then, the visible tokens  $\mathcal{Z}_{vis}$  and the infrared tokens  $\mathcal{Z}_{ir}$  are input to the External Modal Prompt Generator (EMPG) to generate external modal prompts  $\mathcal{P}_E$ , which are fused with the visible tokens in element-wise summation:

$$\mathcal{Z}^0 = \mathcal{Z}_{vis} + \mathcal{P}_E, \quad (2)$$

where  $\mathcal{Z}^0$  is the prompted tokens that contain low-level features from visible and infrared modalities, then it is injected into the first layer of a  $L$ -layer transformer encoder. Here we denote the  $\mathcal{Z}^{l-1}$  as inputs to the  $l$ -th encoder layer  $\mathcal{E}^l$ , and the  $\mathcal{Z}^l$  is the output of  $l$ -th encode layer  $\mathcal{E}^l$ , which is the external modal prompts for the next encoder layer. Formally, the process of the  $l$ -th PVM can be formulated as:

$$\mathcal{Z}^l = \mathcal{E}^l(\mathcal{Z}^{l-1}), \quad l = 1, 2, 3, \dots, L \quad (3)$$

$$\mathbf{p} = \phi(\mathcal{Z}^L), \quad (4)$$

where the transformer encoder layer  $\mathcal{E}^l$  includes Multi-head Self-Attention (MHSA), LayerNorm and Feed-Forward Network (FFN).

Within each encoder layer, we insert the Hybrid Adapter (HA)  $\psi$  to refine the mixed features. Specifically, given input features  $\mathcal{Z}$  from frozen layers, the adapted features  $\mathcal{Z}_\psi$  can be gained by:

$$\mathcal{Z}_\psi = \psi(\mathcal{Z}) + \mathcal{Z}, \quad (5)$$

meanwhile, the external modal prompts  $\mathcal{P}_E$  are input to the Internal Prompt Adapter (IPA) for further feature transformation, then generating internal prompts  $\mathcal{P}_I$ , which are

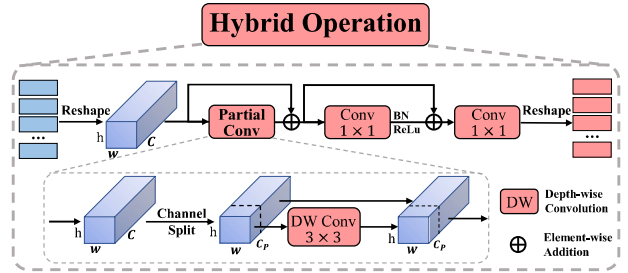


Figure 3. **Detailed design of our Hybrid Operation.** The input tokens are reshaped to feature maps, then a partial convolution is applied, followed by two  $1 \times 1$  convolution layers with batch normalization and ReLU activation in between. We set the split channel  $C_P$  as  $\frac{C}{4}$  by default.

added to adapted feature tokens in element-wise summation:

$$\mathcal{Z}_P = \mathcal{Z}_\psi + \mathcal{P}_I, \quad (6)$$

where  $\mathcal{Z}_P$  is the prompted internal tokens within the encoder layer. Note that we place two sets of {HA, IPA} modules after both the MHSA layer and FFN. The  $\mathcal{Z}_P$  obtained from the second {HA, IPA} module is then input to the next encoder layer of the PVMs.

#### 3.2. External Modal Prompt Generator

In our case, a key challenge is maintaining the effectiveness of inter-modal learning while simplifying the interaction between the infrared and visible modalities. Considering that the visible feature extracted by the PVM has a relatively stable distribution, relying on these robust visible features becomes crucial when there is no specific backbone for learning infrared features. To this end, we propose the External Prompt Generator (EMPG), which integrates visible embedding tokens and infrared embedding tokens to generate external modality prompts  $\mathcal{P}_E$ :

$$\mathcal{P}_E = EMPG(\mathcal{Z}_{vis}, \mathcal{Z}_{ir}). \quad (7)$$

Considering the redundancy in single-modal information and the need to minimize parameters in the fine-tuning module, we project each flow with  $1 \times 1$  convolution layers into a lower dimension  $d_1$  by:

$$\mathcal{M}'_{vis} \in \mathbb{R}^{N \times d_1} = s_1(\mathcal{Z}_{vis}), \quad (8)$$

$$\mathcal{M}'_{ir} \in \mathbb{R}^{N \times d_1} = s_2(\mathcal{Z}_{ir}), \quad (9)$$

where the  $\mathcal{M}'_{vis}$  and  $\mathcal{M}'_{ir}$  are visible and infrared hidden tokens, respectively.

**Hybrid Operation.** Considering that the PVMs are frozen, the downstream visible features are extracted based on the parameterized tendencies of the PVM, which may be insufficient for effective transfer. To address this, we propose the Hybrid Operation, as shown in Fig. 3, stacking



convolution layers to enhance the perceptual dimension of visible features. To minimize parameters, we apply depth-wise convolutions [6] to a subset channels of visible tokens, while two point-wise convolutions further gather information across all channels. Multiple residual connections are incorporated to reduce feature loss.

Meanwhile, as infrared flow has relatively simple features (i.e., it lacks information such as color and texture), simAM [69] is adopted to capture infrared structural feature, which produces the enhanced embeddings  $\mathcal{M}_{ir}^e$  by applying the channel-wise spatial attention weight  $\frac{1}{e_t^*}$  over  $\mathcal{M}_{ir}'$ :

$$\mathcal{M}_{vis}^e = g_h(\mathcal{M}_{vis}'), \quad (10)$$

$$\mathcal{M}_{ir}^e = \mathcal{M}_{ir}' \odot \text{sigmoid}\left(\frac{1}{B}\right), \quad (11)$$

$$e_t^* = \frac{4(\delta^2 + \lambda)}{(t - \hat{\mu})^2 + 2\delta^2 + 2\lambda}, \quad (12)$$

where  $\lambda$  is a hyper parameter,  $t$  is input feature of a single channel,  $\delta^2$  and  $\hat{\mu}$  are the energy factors calculated from input feature,  $B$  groups all  $e_t^*$ , and  $\odot$  is the Hadamard product. Lastly, we obtain mixed modal representations by additive binding, and the learned modal prompts can be gained by:

$$\mathcal{P}_E = s_3(\mathcal{M}_{vis}^e + \mathcal{M}_{ir}^e), \quad (13)$$

where  $s_3(\cdot)$  is the same as  $s_1(\cdot)$  and  $s_2(\cdot)$ .

### 3.3. Hybrid Adapter

For dense prediction tasks, the simple projection of the vanilla adapter is insufficient for transferring visual knowledge [70]. Therefore, we integrate the proposed HO module into the vanilla adapter and additionally introduce the simple feature transform strategy (SFT), to optimize task-agnostic representations from frozen encoder layers

Specifically, given input  $\mathcal{Z}$  from the frozen layers, the output  $\mathcal{Z}'$  of SFT is formulated as:

$$\mathcal{Z}' = LN(\mathcal{Z}) \odot \gamma + \beta, \quad (14)$$

where  $\gamma$  and  $\beta$  are learnable vectors,  $LN$  is the LayerNorm, and  $\odot$  is the Hadamard product. Formally, the output  $\mathcal{Z}_\psi$  of the Hybrid Adapter can be gained by:

$$\mathcal{Z}_\psi = [(GeLu(g_h(SFT(\mathcal{Z})\mathbf{W}_d^T))\mathbf{W}_u^T)], \quad (15)$$

where the  $\mathbf{W}_d \in \mathbb{R}^{r \times d_2}$  and  $\mathbf{W}_u \in \mathbb{R}^{d_2 \times r}$  are the parameters of down-projection and up-projection, respectively, GeLu is the activation function.

### 3.4. Internal Prompt Adapter

Intrinsically, the external modal prompts  $\mathcal{P}_E$  contain low-level features from infrared and visible modalities,

which can be reprocessed to benefit downstream tasks. However, features are highly nonlinearized after multi-layer encoder processing. We found that directly fusing the output of the Hybrid Adapter with external modal prompts  $\mathcal{P}_E$  causes performance degradation due to heterogeneous feature conflicts. To address this, we propose the Internal Prompt Adapter (IPA). As shown in Fig. 2, IPA follows the structure of the vanilla adapter, but unlike HA, it aims to progressively adjust the input distribution of external prompts at each layer, reducing heterogeneous feature conflicts when merging with HA's outputs. Since the external modal prompts are low-level features, we re-use simAm [69] to scale their attention. We found that applying SFT before and after projection improves performance but only introducing an additional 0.3% parameters. The learned internal prompts are added to the output of HA  $\mathcal{Z}_\psi^l$  to gain prompted tokens  $\mathcal{Z}_P^l$  as Eq. (6), which contains mixed blending representation.

### 3.5. Optimization

During the tuning process, we freeze the parameters of PVMs and only optimize a few parameters  $\theta = \{\tau^{ir}, \mathcal{P}_E, \{\mathcal{Z}_\psi^l\}_{l=1}^L, \{\mathcal{P}_I^l\}_{l=1}^L, \theta_d\}$ , where  $\tau^{ir}$  denotes the patch embedding layer of infrared inputs, and  $\theta_d$  is the decoder for specific task. Therefore, the optimization process can be formulated as:

$$\theta_{IV-tuning} = \arg \min_{\theta} \frac{1}{|\mathcal{D}|} \sum \mathcal{L}(\phi(\mathcal{Z}^L, \mathbf{y})), \quad (16)$$

where  $\mathcal{D}$  denotes the downstream infrared-visible data, and  $\mathcal{L}$  denotes the overall loss function of IV-tuning which is the same as that of the full fine-tuning model. For semantic segmentation, we use cross-entropy loss [41] as the loss function; For salient object detection, we follow CPNet [24] to use a hybrid loss composed of BCE loss [8] and IoU loss [44]. For object detection, the loss function can be formulated as:

$$\mathcal{L} = L_{cls} + \lambda_{iou}L_{iou} + \lambda_{L_1}L_1, \quad (17)$$

where  $L_{cls}$  is the weighted focal loss for classification,  $L_1$  and generalized IoU loss  $L_{iou}$  are employed for bounding box regression, with  $\lambda_{iou}$  and  $\lambda_{L_1}$  as the regularization parameters.

## 4. Experiment

### 4.1. Experiment Settings

**IR-VIS Salient Object Detection.** We conduct experiments on three IR-VIS datasets, VT821 [56], VT1000 [58] and VT5000 [59], which contains 821, 1000 and 5000 IR-VIS image pairs, respectively. For fair comparison, we use the training dataset in VT5000, which consists of 2,500 image pairs. The rest image pairs are used for testing. We

Methods	Publications	Backbone	#TP	VT821 [56]				VT1000 [58]				VT5000 [59]			
				$S_\alpha \uparrow$	$F_\beta^\omega \uparrow$	$E_m^a \uparrow$	$MAE \downarrow$	$S_\alpha \uparrow$	$F_\beta^\omega \uparrow$	$E_m^a \uparrow$	$MAE \downarrow$	$S_\alpha \uparrow$	$F_\beta^\omega \uparrow$	$E_m^a \uparrow$	$MAE \downarrow$
SwinNet [40]	TCSVT 22	Swin-B [39]	88.00M	0.904	0.818	0.926	0.030	0.938	0.894	0.947	0.018	0.912	0.846	0.942	0.026
LSNet [80]	TIP 23	MobileNet-v2 [50]	3.40M	0.877	-	0.911	0.033	0.924	0.911	0.022	0.876	-	0.916	0.036	
CAVER [46]	TIP 23	ResNet101 [18]	44.50M	0.898	0.845	-	0.027	0.938	0.911	-	0.017	0.899	0.849	-	0.028
SACNet [63]	TMM 24	Swin-B [39]	88.00M	0.906	0.859	-	0.025	0.942	0.927	-	0.014	0.917	0.888	-	0.021
TCINet [42]	TCE 24	Swin-B [39]	88.00M	0.914	0.872	0.938	0.024	0.942	0.920	0.968	0.015	0.918	0.879	0.949	0.023
ConTriNet [55]	TPAMI 25	Swin-B [39]	88.00M	0.915	0.876	0.940	<b>0.022</b>	0.941	0.924	0.954	0.015	0.923	0.895	0.956	0.020
CPNet [24] (baseline)	IJCV 24	Swin-L [39]	192.50M	0.890	0.831	0.917	0.033	0.939	0.918	0.966	0.015	0.911	0.873	0.949	0.025
<b>+IV-tuning (Ours)</b>	-	Swin-L [39]	6.06M	0.909 (+0.019)	0.859 (+0.028)	0.938 (+0.021)	0.027 (-0.006)	0.941 (+0.002)	0.918 (+0.0)	0.965 (-0.001)	0.015 (-0.0)	0.919 (+0.008)	0.887 (+0.014)	0.959 (+0.010)	0.021 (-0.004)
CPNet [24] (baseline)	IJCV 24	EVA02-L [14]	304.24M	0.890	0.832	0.915	0.034	0.938	0.915	0.959	0.017	0.907	0.866	0.943	0.026
<b>+IV-tuning (Ours)</b>	-	EVA02-L [14]	8.90M	<b>0.923 (+0.033)</b>	<b>0.889 (+0.057)</b>	<b>0.952 (+0.057)</b>	<b>0.022 (-0.012)</b>	<b>0.948 (+0.010)</b>	<b>0.931 (+0.016)</b>	<b>0.975 (+0.016)</b>	<b>0.013 (-0.004)</b>	<b>0.930 (+0.023)</b>	<b>0.904 (+0.038)</b>	<b>0.966 (+0.023)</b>	<b>0.019 (-0.007)</b>

Table 1. Overall performance on the VT821 [56], VT1000 [58] and VT5000 [59] datasets for infrared-visible salient object detection. The trainable parameters in backbones (#TP), S-measure ( $S_\alpha$ ), weighted F-measure ( $F_\beta^\omega$ ), adapted E-measure ( $E_m^a$ ) and mean absolute error ( $MAE$ ) are reported. We use violet color to represent the degree of performance gain compared to full fine-tuning baselines.

Methods	Publications	Backbone	#TP	$mIoU$
RSFNet [32]	ICCV 23	ResNet-18 [18]	11.70M	54.60
CDDFuse [77]	CVPR 23	DeepLab-V3 [4]	42.52M	44.50
CMX [76]	T-ITS 23	Mit-B4 [67]	64.00M	59.70
EAEFNet [34]	RAL 23	ResNet-152 [18]	60.20M	55.40
GoPT [21]	AAAI 24	MAE-L [20]	306.51M	57.70
CAINet [43]	TMM 24	MobileNet-V2 [50]	3.4M	58.60
Segformer (baseline)	NeurIPS 21	EVA02-L [14]	304.24M	54.53
<b>+IV-tuning (Ours)</b>	-	EVA02-L [14]	8.90M (2.93%)	59.56 (+5.03)
Segformer (baseline)	NeurIPS 21	Swin-L [39]	192.50M	56.78
<b>+IV-tuning (Ours)</b>	-	Swin-L [39]	6.06M (3.15%)	<b>60.07 (+3.29)</b>

Table 2. Overall performance on the MFNet [17] dataset for infrared-visible semantic segmentation. The trainable parameters in backbones (#TP) and  $mIoU$  are reported.

Methods	Publications	Backbone	#TP	$mAP$	$mAP@50$	$mAP@75$
TarDAL [37]	CVPR 22	CSPDarknet53 [61]	86.25M	54.5	80.9	-
CDDFuse [77]	CVPR 23	CSPDarknet53 [61]	86.25M	54.6	81.1	57.0
CBAM [9]	WACV 24	EfficientNet [54]	77.00M	50.5	81.0	-
CoCoNet [38]	IJCV 24	CSPDarknet53 [61]	86.25M	54.2	80.7	-
ICAFusion [51]	PR 24	CSPDarknet53 [61]	86.25M	59.9	89.2	65.0
CO-DETR (baseline) [83]	ICCV 23	Swin-L [39]	192.50M	59.5	90.2	62.5
<b>+IV-tuning (Ours)</b>	-	Swin-L [39]	6.06M (3.15%)	<b>61.3 (+1.8)</b>	<b>90.6 (+0.4)</b>	<b>65.2 (+2.7)</b>
DINO (baseline) [74]	ICRL 23	Swin-L [39]	192.50M	60.2	91.1	64.1
<b>+IV-tuning (Ours)</b>	-	Swin-L [39]	6.06M (3.15%)	<b>61.1 (+0.9)</b>	<b>91.9 (+0.8)</b>	<b>66.0 (+1.9)</b>

Table 3. Overall performance on the M3FD [37] dataset for infrared-visible object detection. The trainable parameters in backbones (#TP),  $mAP$ ,  $mAP@50$ , and  $mAP@75$  are reported.

compare our IV-tuning with state-of-the-art infrared-visible methods, including SwinNet [40], LSNet [80], CAVER [46], SACNet [63], TCINet [42] and ConTriNet [55].

**IR-VIS Semantic Segmentation.** MFNet [17] is an commonly used IR-VIS dataset, which has 1569 images annotated in 8 classes. The training and test sets have 1176 and 393 image pairs, respectively. We adopt the mean Intersection over Union ( $mIoU$ ) as the evaluation metric. We compare our IV-tuning with state-of-the-art infrared-visible methods, including CDDFuse [77], RSFNet [32], EAEFNet [34], CMX [76], GoPT [21] and CAINet [43].

**IR-VIS Object Detection.** M3FD [37] is an IR-VIS object detection dataset containing 4,200 image pairs with six categories. The training and test sets have 3,360 and 840 image pairs, respectively. We report the  $mAP$ ,  $mAP50$ , and  $mAP75$  to evaluate the performance. We compare IV-tuning with state-of-the-art infrared-visible methods, including CoCoNet [38], TarDAL [37], CBAM [9], ICAFusion [51], CDDFuse [77] and CFT [49].

**Pre-trained Visual Models.** For salient object detec-

tion and semantic segmentation, we employ Swin Transformer [39] pre-trained on ImageNet-21K [10] and EVA02 [14] pre-trained on the Merged-38M [14] dataset. For a fair comparison in object detection, we only employ Swin Transformer [39] as it is the only transformer-based model that provides COCO pre-trained weights along with transformer-based detectors, which is crucial for overall performance. To balance precision and efficiency, we employ the large version of these architectures. For the decoder, we adopt Segformer [67] in semantic segmentation, CO-DETR [83] and DINO [74] for object detection, and RCM blocks in CPNet [24] for salient object detection, respectively.

**Implementation Details.** We modify the mmsegmentation [7] and mmdetection [3] to support dual-branch image input. To demonstrate the superior performance of IV-tuning in leveraging additional modalities with fewer parameters, we construct the baseline by fully fine-tuning the model using only the visible modality. For salient object detection, we use Adam ( $lr = 5e-5$ , weight decay =  $1e-1$ ) and train for 200 epochs with a batch size of 8 on  $384 \times 384$  cropped images. For semantic segmentation, we use SGD ( $lr = 1e-3$ , weight decay =  $1e-2$ ) and train for 160,000 iterations with a batch size of 2 on  $512 \times 512$  cropped images. For object detection, we use AdamW ( $lr = 1e-4$ , weight decay =  $1e-4$ ) and train for 36 epochs with a batch size of 2 on  $640 \times 640$  cropped images. All experiments follow identical settings for fair comparison. During tuning, only the original PVM parameters are frozen, while the decoder and the IV-tuning components are trainable. By default, the hidden dimensions are set as follows:  $d_1 = 8$  for EMPG,  $d_2 = 64$  for HA, and  $d_3 = 8$  for IPA, with the ablation studies in the Supplementary Material. Benefiting from streamlined architecture and reduced parameters, IV-tuning can fine-tune models like Swin-L [39] or EVA02-L [14] on a single RTX 3090. Details regarding memory usage, storage, etc., are presented in the supplementary material.

## 4.2. IV-tuning on IR-VIS Salient Object Detection.

As shown in Tab. 1, without any special design, the baseline methods that only utilizes the PVM can achieve comparable performance. For example, the baseline method equipped with Swin-L [39] demonstrates competitive per-

Methods	Publications	#TP	MFNet [17]		M3FD [37]	
			Swin-L+Segformer [39, 67]		Swin-L+CO-DETR [39, 83]	
			<i>mIoU</i>	<i>mAcc.</i>	<i>mAP</i>	<i>mAP@75</i>
Full Fine-tune (baseline)	NeurIPS 21	192.50M	56.78	64.88	59.5	62.6
Freeze	-	0.00M	53.02	60.66	56.6	58.2
+VPT [26]	ECCV 22	0.20M	56.79	64.55	60.4	64.4
+AdaptFormer [5]	NeurIPS 22	2.34M	49.79	54.78	60.1	62.8
+Bi-AdaptFormer [28]	ICCV 23	1.16M	58.14	65.28	60.8	63.6
+Rein [65]	CVPR 24	14.72M	57.83	65.07	60.9	64.8
<b>+IV-tuning (Ours)</b>	-	6.06M	<b>60.07</b>	<b>68.00</b>	<b>61.3</b>	<b>65.2</b>

Table 4. Comparisons with PETL methods on the semantic segmentation and object detection.

formance compared with CAVER [46] on the VT1000 [58] dataset when only visible data is used. This indicates that transferring a larger-scale PVM is a promising approach. When introducing infrared auxiliary modality, IV-tuning achieves better performance with only 6.06M trainable backbone parameters. Remarkably, when coupled with EVA02-L [14], IV-tuning significantly outperform previous IR-VIS methods and the full fine-tuning baselines with fewer parameters.

### 4.3. IV-tuning on IR-VIS Semantic Segmentation

As shown in Tab. 2, IV-tuning surpasses the full fine-tuning baselines across multiple PVMs, gaining an improvement of 9.2% and 5.8% when coupled with EVA02-L [14] and Swin-L [39], respectively. This demonstrates that IV-tuning exhibits superior capability in adapting PVMs to downstream tasks. More discussion on the “adaptation” is available in the supplementary material. Besides, our IV-tuning beats all state-of-the-art methods, achieving the highest *mIoU* of **60.07%**. Notably, some methods such as CDDFuse [77] adopt a two-stage training while IV-tuning only fine-tuning approximately 3% of the backbone parameters in one training stage, indicating that IV-tuning is highly efficient and effective.

### 4.4. IV-tuning on IR-VIS Object Detection

As shown in Tab. 3, IV-tuning surpasses the full fine-tuning across two baselines, achieving superior performance with fewer parameters. Notably, benefiting from the supplementary information provided by the infrared modality, IV-tuning achieves improvements of **4.3%** and **3.0%** in *mAP75* on Swin-L+CODETR [39, 83] and Swin-L+DINO [39, 74], respectively. This indicates that IV-tuning effectively leverages the complementary information from visible and infrared modalities, resulting in more precise predictions of object shapes and boundaries under high IoU conditions. Meanwhile, IV-tuning achieves a **2.0%** improvement in *mAP* compared to ICAFusion [51], demonstrating the advantages of IV-tuning in harnessing large-scale PVMs for object detection.

### 4.5. Comparisons with other PETL Methods

To further explore the effectiveness of IV-tuning, we compare it with various Parameter-Efficient Transfer Learn-

ing (PETL) methods, including VPT [26], AdaptFormer [5], Bi-AdaptFormer [28] and Rein [65]. We conduct experiments using Swin-L+Segformer [39, 67] for semantic segmentation and Swin-L+CO-DETR [39, 83] for object detection. We introduce the “Freeze” method to observe the effect of freezing the entire PVMs without adding any new parameters, while only training the task-specific heads. Note that we insert an independent infrared patch embedding layer in PVMs and add the infrared tokens to the visible tokens to get dual-modal results. As shown in Tab. 4, due to the powerful and robust feature extraction capabilities of PVMs, some PETL methods have achieved comparable performance. Most PETL methods outperform the Full Fine-tune and Freeze baselines across both tasks. This indicates that PETL methods are promising and efficient fine-tuning solutions. Tailored for IR-VIS tasks, the proposed IV-tuning achieves even superior performance, surpassing previous PETL methods and full fine-tuning with the same backbone. Visual samples for qualitative comparison are in the Supplementary Material.

### 4.6. Ablation Study

We conduct experiments on semantic segmentation with Segformer [67] and object detection with CO-DETR [83].

**Analysis on each component.** Our IV-tuning consists of three key components: the External Modal Prompt Generator (EMPG), the Hybrid Adapter (HA), and the Internal Prompt Adapter (IPA). As shown in Tab. 5 (a), when no components are included, the “Freeze” setting only achieves a *mIoU* of 53.02% and a *mAP* of 56.6%, respectively. Adding EMPG improves performance by 5.5% *mIoU* and 6.7% *mAP* with merely 0.02M additional parameters. Including HA further boosts performance to 59.91% *mIoU* and 60.5% *mAP*, respectively. We further combine the IPA with the HA to achieve 60.07% and 61.3% performance. Interestingly, IPA shows differences in gains across different tasks, suggesting that exploring its role in feature conflict resolution can be a new direction to explore.

**Analysis on the inserted layers.** Reducing the number of inserted layers can significantly decrease the trainable parameters. As shown in Tab. 5 (b), we observe that the performance consistently improves as the number of inserted layers increases. Moreover, only tuning on shallow or deep layers leads to different performance drops, and tuning the

EMPG	HA	IPA	MFNet [17]		M3FD [37]	
			#TP	mIoU	#TP	mAP
PVMs			Swin-L [39]			
Full fine-tuning			195.20M	56.78	192.50M	61.1
Freeze			0.00M	53.02	0.00M	56.6
✓			0.02M	55.91	0.02M	60.4
✓	✓		5.23M	59.91	5.23M	60.5
✓	✓	✓	6.06M	<b>60.07</b>	6.06M	<b>61.3</b>

(a) Ablation studies on each component.

Layers	MFNet [17]	
	#TP	mIoU
PVMs		
EVA02-L [14]		
1→9	4.18M	59.40
1→14	5.87M	59.55
1→19	7.55M	59.62
6→24	7.55M	60.01
1→24	8.90M	<b>60.07</b>

(b) Ablation studies on inserted layers.

Settings	MFNet [17]		M3FD [37]	
	#TP	mIoU	#TP	mAP
PVMs				
Swin-L [39]				
Parallel	6.06M	47.04	6.06M	56.9
EMPG-Only	0.02M	55.91	0.02M	60.4
MHSA-Only	3.04M	59.25	3.04M	61.1
FFN-Only	3.04M	58.90	3.04M	<b>61.3</b>
IV-tuning	6.06M	<b>60.07</b>	6.06M	<b>61.3</b>

(c) Ablation studies of various variants.

Table 5. Ablation studies on each component, inserted layers, and variants of IV-tuning. The trainable parameters in backbone (#TP), mIoU and mAP are reported.

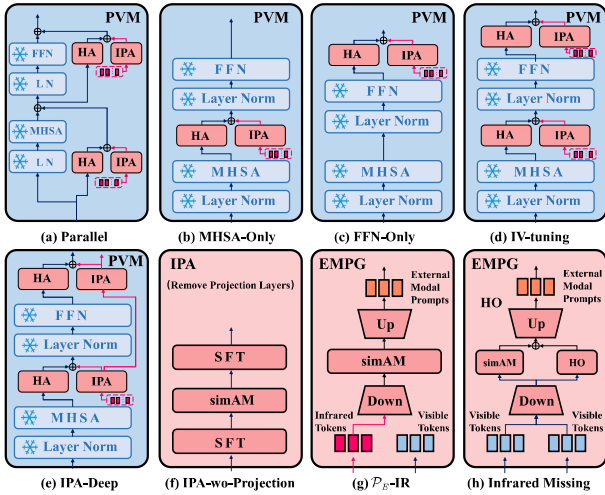


Figure 4. Variants of IV-tuning.

deeper layers that contain high-level semantic information is more helpful for downstream tasks, this has the same tendency as the current common strategy of full fine-tuning the last few layers [72].

**Variants of adapter structure.** We create different variants (See Fig. 4 (a)→(d)), to investigate their impacts. As shown in Tab. 5 (c), when neither HA nor IPA is included (denoted “EMPG-only”), the performance reaches 55.91% and 60.4%. After tuning both the attention layer and the FFN, the “IV-tuning” setting achieves the best performance, demonstrating its effectiveness in enhancing these key transformer components. Additionally, the contributions of attention layer and FFN tuning vary across different tasks. We also found that the parallel structure (Fig. 4 (a)) leads to a significant performance drop, indicating that the sequential architecture is more effective.

**Analysis on the Internal Prompt Adapter, simAM [69] and modalities.** We conduct experiments on two IPA variants to validate key design choices. First, we remove the two projection layers of IPA (Fig. 4 (f)). Without the non-linear effect provided by the projection layer, conflicting features lead to a performance drop (57.74% vs. 59.91%, see Tab. 5 (a), fourth row). This indicates that the non-linear

Settings	MFNet [17]	
	#TP	mIoU
PVMs		
Swin-L [39]		
IPA-wo-Projection	5.45M	57.74
IPA-Deep	6.06M	48.07
wo-simAM [69]	6.06M	59.97
$\mathcal{P}_E$ -IR	6.05M	47.18
IR-Missing	6.06M	55.72

Table 6. Ablation studies on IPA, simAM [69] and modalities.

transformation is effective in alleviating feature conflicts. Next, we explore depth effects by feeding one IPA’s output into the next (Fig. 4 (e)), but this severely degrades performance (48.07% vs. 59.91%), indicating that deeper IPA structures may amplify conflicting features and disrupting feature fusion. In contrast, using independent IPA modules for each layer mitigates this issue and enhances shallow-layer features. We adopt simAM [69], a parameter-free attention module, to enhance early-stage features. As shown in Tab. 6, removing simAM [69] in the EMPG and IPA brings tiny performance drop (59.97% vs. 60.07%), indicating that IV-tuning is highly competitive and does not rely on this specific module. Finally, we conduct experiments with the modality, for example, using only the infrared modality to generate external modal prompts (Fig. 4 (g)) lead to a significant performance degradation (47.18% vs. 60.07%). This indicates that the infrared flow has difficulty learning effective representations when lacking robust visible features as a reference. This verifies the rationality of using dual-modal information to generate prompts, and also justifies our motivation for streamlining the infrared flow based on the robust features of the PVM. We also investigate the performance when the infrared modality is missing by replacing the infrared flow with the visible flow (Fig. 4 (h)). In this case, although IV-tuning falls 1.8% short of full fine-tuning (55.72% vs. 56.78%), it yet highlights the specificity of our design for the infrared modality and its effectiveness in learning complementarity between infrared and visible modalities.



## 5. Conclusion

In this work, we present IV-tuning, a novel parameter-efficient transfer learning method for adapting visible-based Pre-trained Visual Models (PVMs) to IR-VIS tasks, including salient object detection, semantic segmentation and object detection. By streamlining the infrared flow into modal prompts, IV-tuning innovatively excavate the relationship between powerful PVMs and infrared-visible downstream tasks, as well as the complementarity between the infrared and visible modalities. Extensive experiments demonstrate that IV-tuning is effective, efficient, and general in harnessing PVMs across multiple infrared-visible tasks.

# IV-tuning: Parameter-Efficient Transfer Learning for Infrared-Visible Tasks

## Supplementary Material

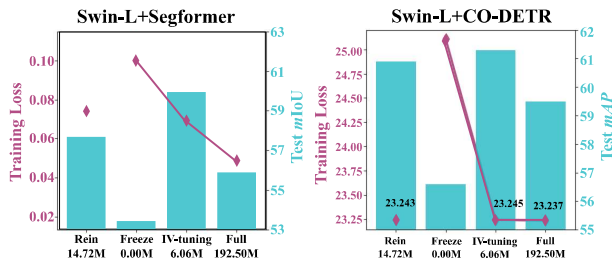


Figure 5. Training loss and test metrics on the MFNet [17] and M3FD [37] datasets, respectively. We use Swin-L+Segformer [39, 67] for semantic segmentation and Swin-L+CO-DETR [39, 83] for object detection, respectively. As the number of training parameters rises (Freeze  $\rightarrow$  IV-tuning  $\rightarrow$  Full), the training loss decreases. However, the metrics on the test set first rise and then fall, reaching a maximum at IV-tuning. This suggests that the full fine-tuning paradigm suffers from overfitting on the dataset, which provides strong evidence for the limitation of full fine-tuning stated in the main paper and further supports our motivation that **streamlining the infrared flow and harnessing PVMs with fewer parameters for superior performance**. Moreover, this phenomenon also applies to the comparison of Rein [65] and IV-tuning, suggesting that our IV-tuning better balances generalizability with the degree of training. The purple line denotes the average training loss when fine-tuned on the MFNet and M3FD datasets, respectively. The blue bars are the test metrics, including  $mIoU$  and  $mAP$ , respectively.

## 6. Training Loss and Test Metrics

Overfitting has been a long-standing concern of researchers. Early neural network research [30] point out that as the training parameters increase, the models are prone to be “Overfitting”. The overfitted models tend to memorize all the data distribution, including the noise, instead of the discipline behind the data. This results in a loss of generalization on the test set.

In order to reduce the effect of overfitting, many solutions are proposed to inhibit the different triggers, such as the early-stopping, network-reduction and training data expansion. However, early stopping is still based on full fine-tuning, which imposes many limitations as mentioned in the main paper. Network pruning for large networks also greatly increases the difficulty of the practice, as it requires fine-tuning different parameters to observe performance changes. The complex acquisition conditions and strict labeling requirements also limit the expansion of dual-modal data. Hence, training with fewer parameters emerges as a feasible strategy for harnessing PVMs for infrared-

visible tasks.

In our main paper, numerous experiments have demonstrated the effectiveness of IV-tuning for adapting PVMs to downstream infrared-visible tasks. We hypothesize that the success of “adaptation” may be due to two factors: 1) *IV-tuning enhances the fitting capability of PVMs, allowing for better alignment with the training data.* 2) *IV-tuning reduces the overfitting of PVMs on small datasets, resulting in improved generalization during testing.* To investigate this, we calculate the average training loss of the last 1,000 iterations in semantic segmentation and that of the last 1 epoch in object detection, respectively, along with their corresponding evaluation metrics. As shown in Fig. 5, as the training parameters increase from Freeze (0.00M)  $\rightarrow$  IV-tuning (6.01M)  $\rightarrow$  Full fine-tuning (Full) (192.50M), the training loss monotonically decreases, suggesting that more trainable parameters can make the model better fit on the training set. However, the test metric increases and decreases, indicating that the full fine-tuning paradigm overfit on the training datasets. This observation aligns with the conclusion in Rein [65], providing strong evidence for the limitation of full fine-tuning discussed in our main paper and supporting our motivation that **streamlining the infrared flow and harnessing PVMs with fewer parameters for superior performance**. Moreover, this phenomenon also applies to the comparison of rein [65] and IV-tuning, indicating that our IV-tuning better balances generalizability with the degree of training.

## 7. Storage and Speed

Our proposed IV-tuning achieves superior performance by fine-tuning approximately 3% of the backbone parameters while significantly reducing training consumption. We present a comparison of training consumption for the experiments involving EVA02-L+Segformer [14, 67] for semantic segmentation, Swin-L+CO-DETR [39, 83] for object detection, and EVA02-I+CPNet [14, 24], as discussed in the main paper. As shown in Tab. 7, compared to the full fine-tuning, IV-tuning reduces the training storage by **62.2%**, **51.9%** and **64.9%** on the MFNet [17], M3FD [37] and VT5000 [59] datasets, respectively. IV-tuning also reduces the GPU memory by 17.1%, 2.4% and 3.8%, respectively. Specifically, for fine-tuning on  $N$  task-oriented datasets, IV-tuning only needs to store one set of the pre-trained parameters and  $N$  sets of the task-specific parameters, significantly reducing the training storage. We believe that as the size of pre-trained models gets larger, storage capacity will become a problem worth considering, whereas

Dataset	PVM-Head	Method	#TP	Storage	GPU Memory
MFNet [17]	EVA02-L+Segformer [14, 67]	Full Fine-tuning	304.24M	3.7 GB	12.8 GB
	EVA02-L+Segformer [14, 67]	IV-tuning	8.90M	1.4 GB	10.6 GB
M3FD [37]	Swin-L+CO-DETR [39, 83]	Full Fine-tuning	192.50M	2.7 GB	16.6 GB
	Swin-L+CO-DETR [39, 83]	IV-tuning	6.06M	1.3 GB	16.2 GB
VT5000 [59]	EVA02-L+CPNet [14, 24]	Full Fine-tuning	304.24M	3.7 GB	23.8 GB
	EVA02-L+CPNet [14, 24]	IV-tuning	8.90M	1.3 GB	22.9 GB

Table 7. Comparison of trainable parameters in backbones (#TP), storage and GPU memory across multiple tasks.

EMPG $d_1$	HA $d_2$	IPA $d_3$	#TP	$mIoU$	$\Delta_{8-64-8}$
8	16	8	2.21M (1.15%)	59.61	-0.7%
8	32	8	3.45M (1.79%)	59.72	-0.5%
8	64	8	6.06M (3.15%)	60.07	-
16	64	16	6.65M (3.45%)	59.27	-1.3%
32	64	32	7.81M (4.06%)	59.45	-1.0%

Table 8. Ablation studies on the hidden dimension of three modules on MFNet [17] Dataset. The trainable parameters in backbones (#TP),  $mIoU$ , and the performance changes relative to the “8-64-8” setting  $\Delta_{8-64-8}$  are reported.

our IV-tuning presents a promising approach to solve it.

## 8. Ablation on the hidden dimension.

In IV-tuning, the three components all project the feature into lower dimensions, which is denoted by  $d_1$  for EMPG,  $d_2$  for HA, and  $d_3$  for IPA. To explore their impact, we conduct a series of combinatorial experiments on the MFNet [17] dataset. For simplicity, the hidden dimensions of EMPG and IPA are the same. As shown in Tab. 8, various parameter changes (2.21M  $\rightarrow$  7.81M) cause only slight performance changes, and the “8-64-8” parameter combination achieves the best performance, which is our default settings of IV-tuning.

## 9. Details of decoder for SOD.

CPNet [24] is an RGB-D salient object detection method. It inserts multi-level cross-modal attention fusion modules (CAM module) into the Swin Transformer to fuse depth and visible features, and inputs the fusion results of the intermediate layers and the final layer into multi-level Residual Convolutional modules (RCM module) to obtain the results. In our solution, we only utilize its multi-level RCM blocks as the SOD decoder.

## 10. Visualization

In this section, we show the prediction results on the VT821 [58], MFNet [17] and M3FD [37] datasets, including PVM-based full fine-tuning, ConTriNet [55], Rein [65],

and our IV-tuning. As shown in Fig. 6, Fig. 7 and Fig. 8, under multiple comparative results, our method outperforms the other methods in terms of accuracy, demonstrating the superior performance of IV-tuning.

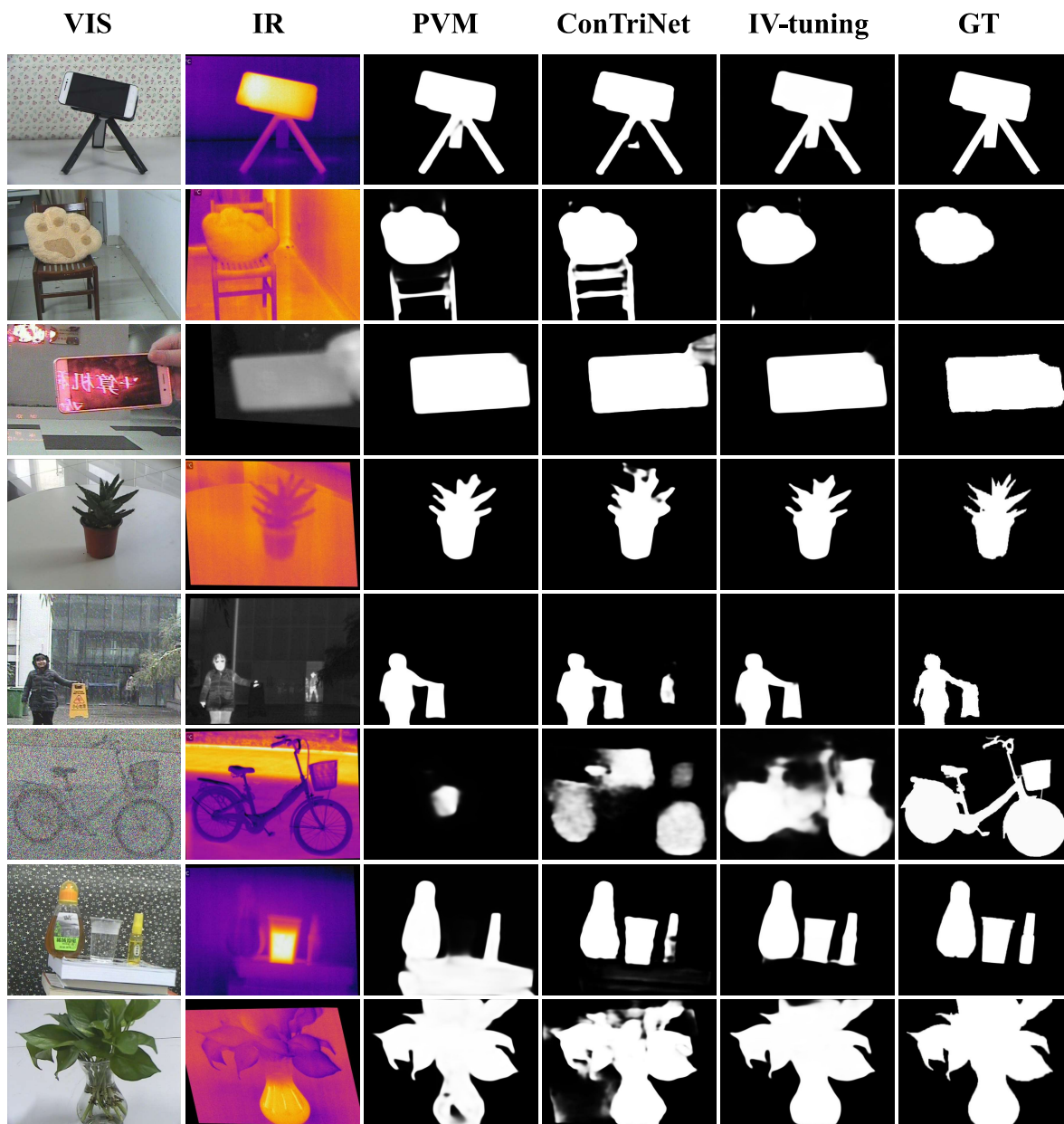


Figure 6. Prediction results of EVA02-L+CPNet [14, 24]+IV-tuning on the VT821 [58] dataset. We show a visual comparison with the Vision Foundation Model fully fine-tuned and ConTriNet [55].



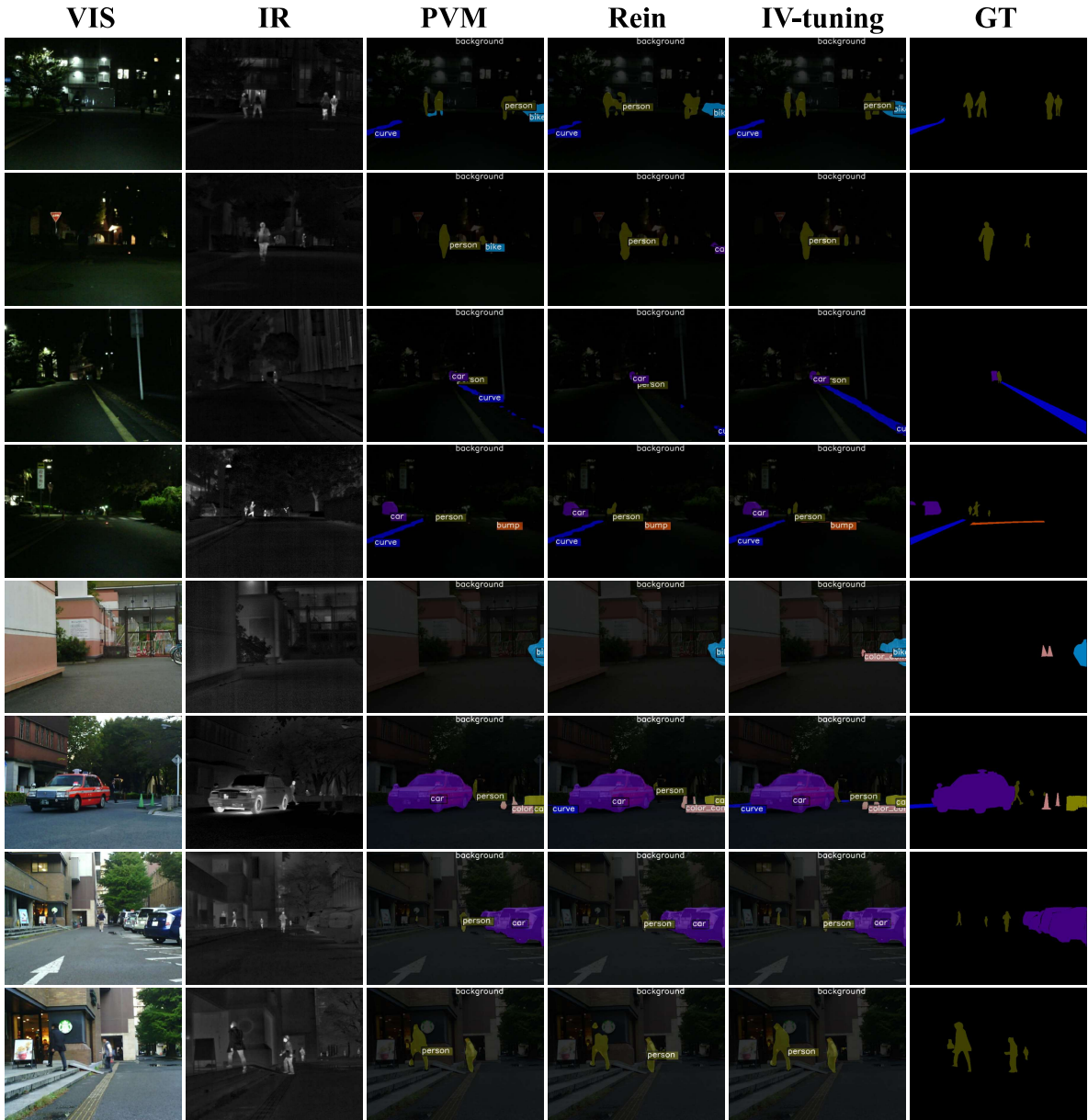


Figure 7. Prediction results of Swin-L+Segformer [39, 67]+IV-tuning on the MFNet [17] dataset. We show a visual comparison with the Pre-trained Visual Model fully fine-tuned and Rein [65].

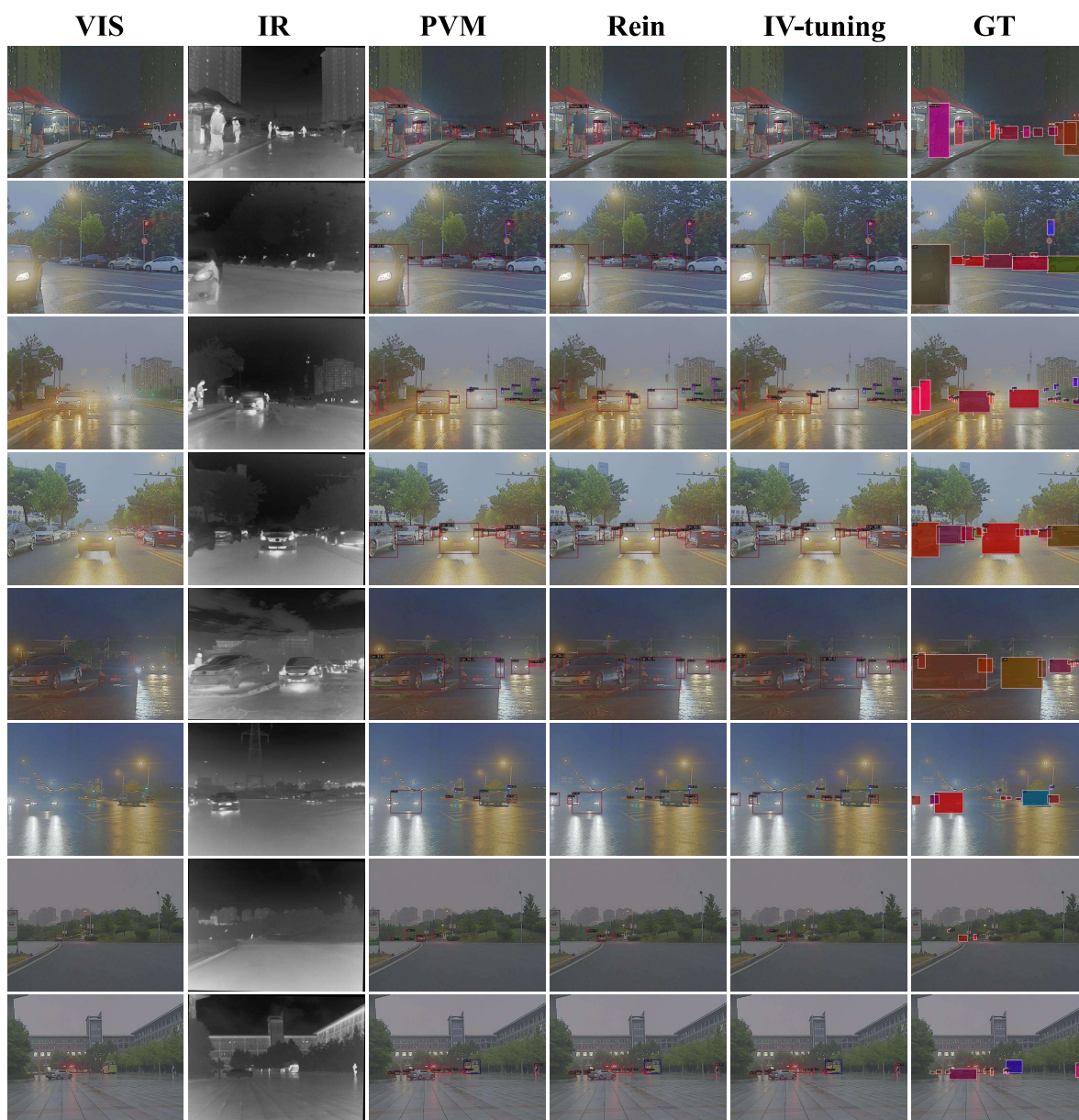


Figure 8. Prediction results of Swin-L+CO-DETR [39, 83] +IV-tuning on the M3FD [37] dataset. We show a visual comparison with the Pre-trained Visual Model fully fine-tuned and Rein [65].

## References

- [1] Alexey Bochkovskiy, Chien-Yao Wang, and Hong-Yuan Mark Liao. Yolov4: Optimal speed and accuracy of object detection. *arXiv preprint arXiv:2004.10934*, 2020. 2
- [2] Rishi Bommasani, Drew A Hudson, Ehsan Adeli, Russ Altman, Simran Arora, Sydney von Arx, Michael S Bernstein, Jeannette Bohg, Antoine Bosselut, Emma Brunskill, et al. On the opportunities and risks of foundation models. *arXiv preprint arXiv:2108.07258*, 2021. 3
- [3] Kai Chen, Jiaqi Wang, Jiangmiao Pang, Yuhang Cao, Yu Xiong, Xiaoxiao Li, Shuyang Sun, Wansen Feng, Ziwei Liu, Jiarui Xu, Zheng Zhang, Dazhi Cheng, Chenchen Zhu, Tianheng Cheng, Qijie Zhao, Buyi Li, Xin Lu, Rui Zhu, Yue Wu, Jifeng Dai, Jingdong Wang, Jianping Shi, Wanli Ouyang, Chen Change Loy, and Dahua Lin. MMDetection: Open mmlab detection toolbox and benchmark. *arXiv preprint arXiv:1906.07155*, 2019. 6
- [4] Liang-Chieh Chen, George Papandreou, Florian Schroff, and Hartwig Adam. Rethinking atrous convolution for semantic image segmentation. *arXiv preprint arXiv:1706.05587*, 2017. 6
- [5] Shoufa Chen, Chongjian Ge, Zhan Tong, Jiangliu Wang, Yibing Song, Jue Wang, and Ping Luo. Adaptformer: Adapting vision transformers for scalable visual recognition. *Advances in Neural Information Processing Systems*, 35:16664–16678, 2022. 2, 3, 7
- [6] François Chollet. Xception: Deep learning with depthwise separable convolutions. In *Proceedings of the IEEE conference on computer vision and pattern recognition*, pages 1251–1258, 2017. 5
- [7] MMSegmentation Contributors. MMSegmentation: Openmmlab semantic segmentation toolbox and benchmark. <https://github.com/open-mmlab/mms Segmentation>, 2020. 6
- [8] Pieter-Tjerk De Boer, Dirk P Kroese, Shie Mannor, and Reuven Y Rubinfeld. A tutorial on the cross-entropy method. *Annals of operations research*, 134:19–67, 2005. 5
- [9] Sri Aditya Deevi, Connor Lee, Lu Gan, Sushruth Nagesh, Gaurav Pandey, and Soon-Jo Chung. Rgb-x object detection via scene-specific fusion modules. In *Proceedings of the IEEE/CVF Winter Conference on Applications of Computer Vision*, pages 7366–7375, 2024. 6
- [10] Jia Deng, Wei Dong, Richard Socher, Li-Jia Li, Kai Li, and Li Fei-Fei. Imagenet: A large-scale hierarchical image database. In *2009 IEEE conference on computer vision and pattern recognition*, pages 248–255. Ieee, 2009. 2, 3, 6
- [11] Jesse Dodge, Gabriel Ilharco, Roy Schwartz, Ali Farhadi, Hannaneh Hajishirzi, and Noah Smith. Fine-tuning pre-trained language models: Weight initializations, data orders, and early stopping. *arXiv preprint arXiv:2002.06305*, 2020. 2
- [12] Alexey Dosovitskiy. An image is worth 16x16 words: Transformers for image recognition at scale. *arXiv preprint arXiv:2010.11929*, 2020. 2, 3
- [13] Siqi Fan, Zhe Wang, Yan Wang, and Jingjing Liu. Spidmesh: Spatial-aware demand-guided recursive meshing for rgb-t semantic segmentation. *arXiv preprint arXiv:2303.08692*, 2023. 2
- [14] Yuxin Fang, Quan Sun, Xinggong Wang, Tiejun Huang, Xinlong Wang, and Yue Cao. Eva-02: A visual representation for neon genesis. *Image and Vision Computing*, 149:105171, 2024. 2, 3, 6, 7, 8, 1
- [15] Zhen Feng, Yanning Guo, and Yuxiang Sun. Cekd: Cross-modal edge-privileged knowledge distillation for semantic scene understanding using only thermal images. *IEEE Robotics and Automation Letters*, 8(4):2205–2212, 2023. 3
- [16] Junjie Guo, Chenqiang Gao, Fangcen Liu, Deyu Meng, and Xinbo Gao. Damsdet: Dynamic adaptive multispectral detection transformer with competitive query selection and adaptive feature fusion. *ECCV*, 2024. 2, 3
- [17] Qishen Ha, Kohei Watanabe, Takumi Karasawa, Yoshitaka Ushiku, and Tatsuya Harada. Mfnet: Towards real-time semantic segmentation for autonomous vehicles with multispectral scenes. In *2017 IEEE/RSJ International Conference on Intelligent Robots and Systems (IROS)*, pages 5108–5115. IEEE, 2017. 6, 7, 8, 1, 2, 4
- [18] Kaiming He, Xiangyu Zhang, Shaoqing Ren, and Jian Sun. Deep residual learning for image recognition. In *Proceedings of the IEEE conference on computer vision and pattern recognition*, pages 770–778, 2016. 2, 3, 6
- [19] Kaiming He, Georgia Gkioxari, Piotr Dollár, and Ross Girshick. Mask r-cnn. In *Proceedings of the IEEE international conference on computer vision*, pages 2961–2969, 2017. 2
- [20] Kaiming He, Xinlei Chen, Saining Xie, Yanghao Li, Piotr Dollár, and Ross Girshick. Masked autoencoders are scalable vision learners. In *Proceedings of the IEEE/CVF conference on computer vision and pattern recognition*, pages 16000–16009, 2022. 3, 6
- [21] Qibin He. Prompting multi-modal image segmentation with semantic grouping. In *Proceedings of the AAAI conference on artificial intelligence*, pages 2094–2102, 2024. 6
- [22] Xiuquan Hou, Meiqin Liu, Senlin Zhang, Ping Wei, and Badong Chen. Saliency detr: Enhancing detection transformer with hierarchical saliency filtering refinement. In *Proceedings of the IEEE/CVF Conference on Computer Vision and Pattern Recognition*, pages 17574–17583, 2024. 1
- [23] Andrew G Howard, Menglong Zhu, Bo Chen, Dmitry Kalenichenko, Weijun Wang, Tobias Weyand, Marco Andreetto, and Hartwig Adam. Mobilenets: Efficient convolutional neural networks for mobile vision applications. *arXiv preprint arXiv:1704.04861*, 2017. 3
- [24] Xihang Hu, Fuming Sun, Jing Sun, Fasheng Wang, and Haojie Li. Cross-modal fusion and progressive decoding network for rgb-d salient object detection. *International Journal of Computer Vision*, pages 1–19, 2024. 5, 6, 1, 2, 3
- [25] Gao Huang, Zhuang Liu, Laurens Van Der Maaten, and Kilian Q Weinberger. Densely connected convolutional networks. In *Proceedings of the IEEE conference on computer vision and pattern recognition*, pages 4700–4708, 2017. 3
- [26] Menglin Jia, Luming Tang, Bor-Chun Chen, Claire Cardie, Serge Belongie, Bharath Hariharan, and Ser-Nam Lim. Visual prompt tuning. In *European Conference on Computer Vision*, pages 709–727. Springer, 2022. 2, 3, 7



- [27] Lihua Jian, Songlei Xiong, Han Yan, Xiaoguang Niu, Shaowu Wu, and Di Zhang. Rethinking cross-attention for infrared and visible image fusion. *arXiv preprint arXiv:2401.11675*, 2024. 3
- [28] Shibo Jie, Haoqing Wang, and Zhi-Hong Deng. Revisiting the parameter efficiency of adapters from the perspective of precision redundancy. In *Proceedings of the IEEE/CVF International Conference on Computer Vision*, pages 17217–17226, 2023. 7
- [29] Muhammad Uzair Khattak, Hanoona Rasheed, Muhammad Maaz, Salman Khan, and Fahad Shahbaz Khan. Maple: Multi-modal prompt learning. In *Proceedings of the IEEE/CVF Conference on Computer Vision and Pattern Recognition*, pages 19113–19122, 2023. 2, 3
- [30] Steve Lawrence, C Lee Giles, and Ah Chung Tsoi. Lessons in neural network training: Overfitting may be harder than expected. In *Aaai/aaai*, pages 540–545, 1997. 1
- [31] Minglei Li, Peng Ye, Yongqi Huang, Lin Zhang, Tao Chen, Tong He, Jiayuan Fan, and Wanli Ouyang. Adapter-x: A novel general parameter-efficient fine-tuning framework for vision. *arXiv preprint arXiv:2406.03051*, 2024. 2, 3
- [32] Ping Li, Junjie Chen, Binbin Lin, and Xianghua Xu. Residual spatial fusion network for rgb-thermal semantic segmentation. *Neurocomputing*, 595:127913, 2024. 2, 3, 6
- [33] Qing Li, Changqing Zhang, Qinghua Hu, Pengfei Zhu, Huazhu Fu, and Lei Chen. Stabilizing multispectral pedestrian detection with evidential hybrid fusion. *IEEE Transactions on Circuits and Systems for Video Technology*, 2023. 3
- [34] Mingjian Liang, Junjie Hu, Chenyu Bao, Hua Feng, Fuqin Deng, and Tin Lun Lam. Explicit attention-enhanced fusion for rgb-thermal perception tasks. *IEEE Robotics and Automation Letters*, 8(7):4060–4067, 2023. 6
- [35] Zhiqiu Lin, Samuel Yu, Zhiyi Kuang, Deepak Pathak, and Deva Ramanan. Multimodality helps unimodality: Cross-modal few-shot learning with multimodal models. In *Proceedings of the IEEE/CVF Conference on Computer Vision and Pattern Recognition*, pages 19325–19337, 2023. 3
- [36] Fangcen Liu, Chenqiang Gao, Yaming Zhang, Junjie Guo, Jinhao Wang, and Deyu Meng. Infmae: A foundation model in infrared modality. *ECCV*, 2024. 2, 3
- [37] Jinyuan Liu, Xin Fan, Zhanbo Huang, Guanyao Wu, Risheng Liu, Wei Zhong, and Zhongxuan Luo. Target-aware dual adversarial learning and a multi-scenario multi-modality benchmark to fuse infrared and visible for object detection. In *Proceedings of the IEEE/CVF Conference on Computer Vision and Pattern Recognition*, pages 5802–5811, 2022. 2, 6, 7, 8, 1, 5
- [38] Jinyuan Liu, Runjia Lin, Guanyao Wu, Risheng Liu, Zhongxuan Luo, and Xin Fan. Coconet: Coupled contrastive learning network with multi-level feature ensemble for multi-modality image fusion. *International Journal of Computer Vision*, pages 1–28, 2023. 2, 6
- [39] Ze Liu, Yutong Lin, Yue Cao, Han Hu, Yixuan Wei, Zheng Zhang, Stephen Lin, and Baining Guo. Swin transformer: Hierarchical vision transformer using shifted windows. In *Proceedings of the IEEE/CVF international conference on computer vision*, pages 10012–10022, 2021. 2, 3, 6, 7, 8, 1, 4, 5
- [40] Zhengyi Liu, Yacheng Tan, Qian He, and Yun Xiao. Swinnet: Swin transformer drives edge-aware rgb-d and rgb-t salient object detection. *IEEE Transactions on Circuits and Systems for Video Technology*, 32(7):4486–4497, 2021. 2, 3, 6
- [41] Jonathan Long, Evan Shelhamer, and Trevor Darrell. Fully convolutional networks for semantic segmentation. In *Proceedings of the IEEE conference on computer vision and pattern recognition*, pages 3431–3440, 2015. 5
- [42] Chengtao Lv, Xiaofei Zhou, Bin Wan, Shuai Wang, Yaoqi Sun, Jiyong Zhang, and Chenggang Yan. Transformer-based cross-modal integration network for rgb-t salient object detection. *IEEE Transactions on Consumer Electronics*, 2024. 6
- [43] Ying Lv, Zhi Liu, and Gongyang Li. Context-aware interaction network for rgb-t semantic segmentation. *IEEE Transactions on Multimedia*, 26:6348–6360, 2024. 6
- [44] Gellért Mátyus, Wenjie Luo, and Raquel Urtasun. Deeproadmapper: Extracting road topology from aerial images. In *Proceedings of the IEEE international conference on computer vision*, pages 3438–3446, 2017. 5
- [45] Maxime Oquab, Timothée Darcet, Théo Moutakanni, Huy Vo, Marc Szafraniec, Vasil Khalidov, Pierre Fernandez, Daniel Haziza, Francisco Massa, Alaaeldin El-Nouby, et al. Dinov2: Learning robust visual features without supervision. *arXiv preprint arXiv:2304.07193*, 2023. 2
- [46] Youwei Pang, Xiaoqi Zhao, Lihe Zhang, and Huchuan Lu. Caver: Cross-modal view-mixed transformer for bi-modal salient object detection. *IEEE Transactions on Image Processing*, 32:892–904, 2023. 6, 7
- [47] Wenjie Pei, Tongqi Xia, Fanglin Chen, Jinsong Li, Jiandong Tian, and Guangming Lu. Sa<sup>2</sup>vp: Spatially aligned-and-adapted visual prompt. In *Proceedings of the AAAI Conference on Artificial Intelligence*, pages 4450–4458, 2024. 2, 3
- [48] Matthew E Peters, Sebastian Ruder, and Noah A Smith. To tune or not to tune? adapting pretrained representations to diverse tasks. *arXiv preprint arXiv:1903.05987*, 2019. 2
- [49] Fang Qingyun, Han Dapeng, and Wang Zhaokui. Cross-modality fusion transformer for multispectral object detection. *arXiv preprint arXiv:2111.00273*, 2021. 2, 6
- [50] Mark Sandler, Andrew Howard, Menglong Zhu, Andrey Zhmoginov, and Liang-Chieh Chen. Mobilenetv2: Inverted residuals and linear bottlenecks. In *Proceedings of the IEEE conference on computer vision and pattern recognition*, pages 4510–4520, 2018. 6
- [51] Jifeng Shen, Yifei Chen, Yue Liu, Xin Zuo, Heng Fan, and Wankou Yang. Icafusion: Iterative cross-attention guided feature fusion for multispectral object detection. *Pattern Recognition*, 145:109913, 2024. 2, 3, 6, 7
- [52] Karen Simonyan and Andrew Zisserman. Very deep convolutional networks for large-scale image recognition. *arXiv preprint arXiv:1409.1556*, 2014. 2, 3
- [53] Kechen Song, Liming Huang, Aojun Gong, and Yunhui Yan. Multiple graph affinity interactive network and a variable illumination dataset for rgbt image salient object detection.



- IEEE Transactions on Circuits and Systems for Video Technology*, 33(7):3104–3118, 2022. 1
- [54] Mingxing Tan and Quoc Le. Efficientnet: Rethinking model scaling for convolutional neural networks. In *International conference on machine learning*, pages 6105–6114. PMLR, 2019. 3, 6
- [55] Hao Tang, Zechao Li, Dong Zhang, Shengfeng He, and Jinhui Tang. Divide-and-conquer: Confluent triple-flow network for rgb-t salient object detection. *IEEE Transactions on Pattern Analysis and Machine Intelligence*, 2024. 2, 6, 3
- [56] Jin Tang, Dongzhe Fan, Xiaoxiao Wang, Zhengzheng Tu, and Chenglong Li. Rgbt salient object detection: Benchmark and a novel cooperative ranking approach. *IEEE Transactions on Circuits and Systems for Video Technology*, 30(12):4421–4433, 2019. 5, 6
- [57] Linfeng Tang, Jiteng Yuan, Hao Zhang, Xingyu Jiang, and Jiayi Ma. Piafusion: A progressive infrared and visible image fusion network based on illumination aware. *Information Fusion*, 2022. 2
- [58] Zhengzheng Tu, Tian Xia, Chenglong Li, Xiaoxiao Wang, Yan Ma, and Jin Tang. Rgb-t image saliency detection via collaborative graph learning. *IEEE Transactions on Multimedia*, 22(1):160–173, 2019. 5, 6, 7, 2, 3
- [59] Zhengzheng Tu, Yan Ma, Zhun Li, Chenglong Li, Jieming Xu, and Yongtao Liu. Rgbt salient object detection: A large-scale dataset and benchmark. *IEEE Transactions on Multimedia*, 25:4163–4176, 2022. 5, 6, 1, 2
- [60] Ashish Vaswani, Noam Shazeer, Niki Parmar, Jakob Uszkoreit, Llion Jones, Aidan N Gomez, Łukasz Kaiser, and Illia Polosukhin. Attention is all you need. *Advances in neural information processing systems*, 30, 2017. 2, 3
- [61] Chien-Yao Wang, Hong-Yuan Mark Liao, Yueh-Hua Wu, Ping-Yang Chen, Jun-Wei Hsieh, and I-Hau Yeh. Cspnet: A new backbone that can enhance learning capability of cnn. In *Proceedings of the IEEE/CVF conference on computer vision and pattern recognition workshops*, pages 390–391, 2020. 6
- [62] Chien-Yao Wang, Alexey Bochkovskiy, and Hong-Yuan Mark Liao. Yolov7: Trainable bag-of-freebies sets new state-of-the-art for real-time object detectors. In *Proceedings of the IEEE/CVF conference on computer vision and pattern recognition*, pages 7464–7475, 2023. 1
- [63] Kunpeng Wang, Danying Lin, Chenglong Li, Zhengzheng Tu, and Bin Luo. Alignment-free rgbt salient object detection: Semantics-guided asymmetric correlation network and a unified benchmark. *IEEE Transactions on Multimedia*, 2024. 6
- [64] Ziyu Wang, Yanjie Ze, Yifei Sun, Zhecheng Yuan, and Huazhe Xu. Generalizable visual reinforcement learning with segment anything model. *arXiv preprint arXiv:2312.17116*, 2023. 3
- [65] Zhixiang Wei, Lin Chen, Yi Jin, Xiaoxiao Ma, Tianle Liu, Pengyang Ling, Ben Wang, Huaian Chen, and Jinjin Zheng. Stronger fewer & superior: Harnessing vision foundation models for domain generalized semantic segmentation. In *Proceedings of the IEEE/CVF Conference on Computer Vision and Pattern Recognition*, pages 28619–28630, 2024. 1, 3, 7, 2, 4, 5
- [66] Zongwei Wu, Jingjing Wang, Zhuyun Zhou, Zhaochong An, Qiuping Jiang, Cédric Demonceaux, Guolei Sun, and Radu Timofte. Object segmentation by mining cross-modal semantics. In *Proceedings of the 31st ACM International Conference on Multimedia*, pages 3455–3464, 2023. 3
- [67] Enze Xie, Wenhai Wang, Zhiding Yu, Anima Anandkumar, Jose M Alvarez, and Ping Luo. Segformer: Simple and efficient design for semantic segmentation with transformers. *Advances in neural information processing systems*, 34:12077–12090, 2021. 6, 7, 1, 2, 4
- [68] Saining Xie, Ross Girshick, Piotr Dollár, Zhuowen Tu, and Kaiming He. Aggregated residual transformations for deep neural networks. In *Proceedings of the IEEE conference on computer vision and pattern recognition*, pages 1492–1500, 2017. 3
- [69] Lingxiao Yang, Ru-Yuan Zhang, Lida Li, and Xiaohua Xie. Simam: A simple, parameter-free attention module for convolutional neural networks. In *International conference on machine learning*, pages 11863–11874. PMLR, 2021. 5, 8
- [70] Dongshuo Yin, Leyi Hu Bin Li, and Youqun Zhang. Adapter is all you need for tuning visual tasks. *arXiv preprint arXiv:2311.15010*, 2023. 5
- [71] Dongshuo Yin, Yiran Yang, Zhechao Wang, Hongfeng Yu, Kaiwen Wei, and Xian Sun. 1% vs 100%: Parameter-efficient low rank adapter for dense predictions. In *Proceedings of the IEEE/CVF Conference on Computer Vision and Pattern Recognition*, pages 20116–20126, 2023. 3
- [72] Jason Yosinski, Jeff Clune, Yoshua Bengio, and Hod Lipson. How transferable are features in deep neural networks? *Advances in neural information processing systems*, 27, 2014. 8
- [73] Xiaohua Zhai, Alexander Kolesnikov, Neil Houlsby, and Lucas Beyer. Scaling vision transformers. In *Proceedings of the IEEE/CVF conference on computer vision and pattern recognition*, pages 12104–12113, 2022. 3
- [74] Hao Zhang, Feng Li, Shilong Liu, Lei Zhang, Hang Su, Jun Zhu, Lionel M Ni, and Heung-Yeung Shum. Dino: Detr with improved denoising anchor boxes for end-to-end object detection. *arXiv preprint arXiv:2203.03605*, 2022. 6, 7
- [75] Hao Zhang, Feng Li, Huaizhe Xu, Shijia Huang, Shilong Liu, Lionel M Ni, and Lei Zhang. Mp-former: Mask-piloted transformer for image segmentation. In *Proceedings of the IEEE/CVF Conference on Computer Vision and Pattern Recognition*, pages 18074–18083, 2023. 1
- [76] Jiaming Zhang, Huayao Liu, Kailun Yang, Xinxin Hu, Ruiping Liu, and Rainer Stiefelhagen. Cmx: Cross-modal fusion for rgb-x semantic segmentation with transformers. *IEEE Transactions on intelligent transportation systems*, 2023. 6
- [77] Zixiang Zhao, Haowen Bai, Jianshe Zhang, Yulun Zhang, Shuang Xu, Zudi Lin, Radu Timofte, and Luc Van Gool. Cddfuse: Correlation-driven dual-branch feature decomposition for multi-modality image fusion. In *Proceedings of the IEEE/CVF conference on computer vision and pattern recognition*, pages 5906–5916, 2023. 2, 3, 6, 7
- [78] Zixiang Zhao, Haowen Bai, Jianshe Zhang, Yulun Zhang, Kai Zhang, Shuang Xu, Dongdong Chen, Radu Timofte, and Luc Van Gool. Equivariant multi-modality image fusion. In

- Proceedings of the IEEE/CVF Conference on Computer Vision and Pattern Recognition*, pages 25912–25921, 2024. [2](#)
- [79] Wujie Zhou, Qinling Guo, Jingsheng Lei, Lu Yu, and Jenq-Neng Hwang. Ecffnet: Effective and consistent feature fusion network for rgb-t salient object detection. *IEEE Transactions on Circuits and Systems for Video Technology*, 32(3): 1224–1235, 2021. [1](#)
- [80] Wujie Zhou, Yun Zhu, Jingsheng Lei, Rongwang Yang, and Lu Yu. Lsnet: Lightweight spatial boosting network for detecting salient objects in rgb-thermal images. *IEEE Transactions on Image Processing*, 32:1329–1340, 2023. [6](#)
- [81] Xin Zhou, Dingkang Liang, Wei Xu, Xingkui Zhu, Yihan Xu, Zhikang Zou, and Xiang Bai. Dynamic adapter meets prompt tuning: Parameter-efficient transfer learning for point cloud analysis. In *Proceedings of the IEEE/CVF Conference on Computer Vision and Pattern Recognition*, pages 14707–14717, 2024. [2](#)
- [82] Jiawen Zhu, Simiao Lai, Xin Chen, Dong Wang, and Huchuan Lu. Visual prompt multi-modal tracking. In *Proceedings of the IEEE/CVF conference on computer vision and pattern recognition*, pages 9516–9526, 2023. [3](#), [4](#)
- [83] Zhuofan Zong, Guanglu Song, and Yu Liu. Detrs with collaborative hybrid assignments training. In *Proceedings of the IEEE/CVF international conference on computer vision*, pages 6748–6758, 2023. [1](#), [6](#), [7](#), [2](#), [5](#)